

## Dynamo efficiency controlled by hydrodynamic bistability

Sophie Miralles, Johann Herault, Stephan Fauve, Christophe Gissinger, François Pétrélis, François Daviaud, Bérengère Dubrulle, Jean Boisson, Mickaël Bourgoïn, Gautier Verhille, et al.

### ► To cite this version:

Sophie Miralles, Johann Herault, Stephan Fauve, Christophe Gissinger, François Pétrélis, et al.. Dynamo efficiency controlled by hydrodynamic bistability. *Physical Review E: Statistical, Non-linear, and Soft Matter Physics*, American Physical Society, 2014, 89, pp.63023. <10.1103/PhysRevE.89.063023>. <cea-01490850>

HAL Id: cea-01490850

<https://hal-cea.archives-ouvertes.fr/cea-01490850>

Submitted on 16 Mar 2017

**HAL** is a multi-disciplinary open access archive for the deposit and dissemination of scientific research documents, whether they are published or not. The documents may come from teaching and research institutions in France or abroad, or from public or private research centers.

L'archive ouverte pluridisciplinaire **HAL**, est destinée au dépôt et à la diffusion de documents scientifiques de niveau recherche, publiés ou non, émanant des établissements d'enseignement et de recherche français ou étrangers, des laboratoires publics ou privés.

**Dynamo efficiency controlled by hydrodynamic bistability**

Sophie Miralles,<sup>1</sup> Johann Herault,<sup>2</sup> Stephan Fauve,<sup>2</sup> Christophe Gissinger,<sup>2</sup> François Pétrélis,<sup>2</sup> François Daviaud,<sup>3</sup>  
Bérengère Dubrulle,<sup>3</sup> Jean Boisson,<sup>4</sup> Mickaël Bourgoïn,<sup>5</sup> Gautier Verhille,<sup>6</sup> Philippe Odier,<sup>1</sup>  
Jean-François Pinton,<sup>1</sup> and Nicolas Plihon<sup>1</sup>

<sup>1</sup>Laboratoire de Physique, École Normale Supérieure de Lyon, CNRS & Université de Lyon, 46 allée d'Italie, 69364 Lyon Cedex 07, France

<sup>2</sup>Laboratoire de Physique Statistique, École Normale Supérieure, CNRS, Université P. et M. Curie, Université Paris Diderot, Paris, France

<sup>3</sup>SPHYNX, Service de Physique de l'État Condensé, CNRS & CEA Saclay, 91191 Gif-sur-Yvette Cedex, France

<sup>4</sup>Unité de Mécanique (chaire AREVA), ENSTA-ParisTech, 828 Boulevard des Marchaux, 91762 Palaiseau Cedex, France

<sup>5</sup>Laboratoire des Écoulements Géophysiques et Industriels, CNRS & Université Joseph Fourier, BP 53, F-38041 Grenoble cedex 9, France

<sup>6</sup>Institut de Recherche sur les Phénomènes Hors Équilibre, CNRS & Université d'Aix-Marseille,

49 rue F. Joliot Curie, B.P. 146 13384 Marseille cedex 13, France

(Received 10 October 2013; published 30 June 2014; corrected 8 July 2014)

Hydrodynamic and magnetic behaviors in a modified experimental setup of the von Kármán sodium flow—where one disk has been replaced by a propeller—are investigated. When the rotation frequencies of the disk and the propeller are different, we show that the fully turbulent hydrodynamic flow undergoes a global bifurcation between two configurations. The bistability of these flow configurations is associated with the dynamics of the central shear layer. The bistable flows are shown to have different dynamo efficiencies; thus for a given rotation rate of the soft-iron disk, two distinct magnetic behaviors are observed depending on the flow configuration. The hydrodynamic transition controls the magnetic field behavior, and bifurcations between high and low magnetic field branches are investigated.

DOI: [10.1103/PhysRevE.89.063023](https://doi.org/10.1103/PhysRevE.89.063023)

PACS number(s): 47.65.-d, 47.20.Ky, 05.45.-a

**I. INTRODUCTION**

Transitions and multiple stability of highly turbulent flows are ubiquitous in geophysical and astrophysical flows as well as in laboratory experiments. Hydrodynamic multistability has for instance been observed in oceanic currents [1], in tornadoes [2], and in confined laboratory turbulent flows—as global bifurcations in von Kármán flows [3–6], Rayleigh-Bénard convection [7] or bistability in spherical Couette flows [8]. The influence of turbulent fluctuations on these transitions remains an open question. The generation of magnetic fields in astrophysical objects, attributed to the dynamo effect—an instability converting kinetic energy into magnetic energy—occurs through a bifurcation taking place over a turbulent background. Several scenarios for this magnetohydrodynamic (MHD) bifurcation have been proposed. Among them, subcritical bifurcations have been proposed in rotating convective MHD flows [9], with a weak field branch coexisting with a strong field solution when the Lorentz force balances the Coriolis force. Subcritical dynamo bifurcations have been observed in MHD simulations of thermal convection in rotating spheres [10–13], periodic flows [14,15], or Keplerian flows [16]. It was observed in numerical simulations of the Taylor-Green flow that spontaneous bifurcations of the mean flow lead to different dynamo mechanisms [17]. In experiments, the dynamo instability usually develops through continuous supercritical bifurcations, as in the Riga experiment [18], the Karlsruhe experiment [19], and the von Kármán sodium (VKS) experiment [20]. In the latter, bistability between oscillatory and steady dynamo states has also been reported, without any noticeable modifications of the flow [21]; the dynamics was interpreted as resulting from the interaction of two magnetic modes [22]. In a modified setup, we report a global subcritical bifurcation between two turbulent hydrodynamic flow configurations, and show that it results in bistability between low magnetic field and

high magnetic field branches. The link between turbulent hydrodynamic and dynamo bifurcations is also reported here.

**II. EXPERIMENTAL SETUP**

We consider a modified version of the von Kármán sodium experiment shown in Fig. 1. Liquid sodium is set into motion by the counter rotation of a soft-iron disk fitted with blades (at rotation rate  $F_d$ ) and a stainless steel propeller (at rotation rate  $F_p$ ) within a cylindrical container. Following the  $s_n t_m$  notation [23], the mean flow has an “ $s_1 t_2$ ” geometry when  $F_d \sim F_p$ , and an “ $s_1 t_1$ ” geometry when  $F_d = 0$  and  $F_p > 0$ , (“ $s_n t_m$ ” denoting an  $s_n t_m$ -like flow in cylindrical geometry). This study thus complements several investigations on dynamo capacities of  $s_n t_m$  and “ $s_n t_m$ ” flows [24–26] with  $n, m \in \{1, 2\}$ .

The cylindrical container has radius  $R_o = 289$  mm and length 524 mm. The disk is located at  $x = -185$  mm, its radius is  $R_d = 154.5$  mm; and it is fitted with 41-mm-high curved blades. The propeller's radius is  $R_p = 115$  mm and is set at  $x = +100$  mm. The eight propeller blades are 40 mm in height and are tilted by  $30^\circ$  relative to the  $x$  axis (resulting in a ratio of the poloidal to the toroidal flows of order unity, as measured in a water tank [27]). The flow is driven up to typically  $F_d \sim 25$  Hz and  $F_p \sim 48$  Hz by motors with 300 kW available power. Oil circulation in the outer copper cylinder regulates the sodium temperature around  $120^\circ\text{C}$ . The integral kinetic Reynolds number of the flow is in excess of  $10^6$ , i.e., the flows are always highly turbulent.

The torques imparted to the disk ( $\Gamma_d$ ) and propeller ( $\Gamma_p$ ) are measured from FGP CD1120 torque meters. A local miniature potential probe implemented as in [28] is inserted in the midplane of the cylinder, at location V ( $\{x, y, z\} = \{0, 0, -206\}$  mm). It gives access to the azimuthal component  $v_\theta$  of the velocity. Magnetic field measurements are made using arrays of ten, three-axis Hall sensors inserted in radial shafts.

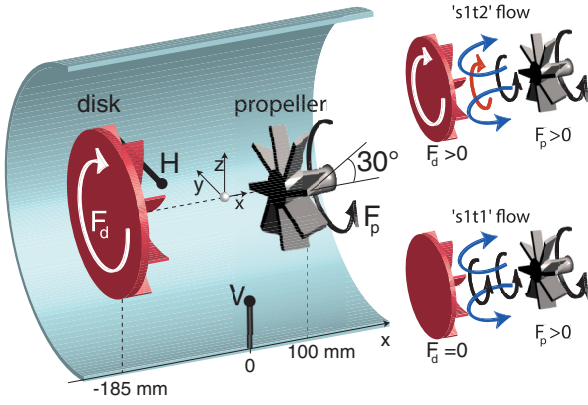


FIG. 1. (Color online) Left: Experimental setup; arrows showing the rotation for positive  $F_d$  and  $F_p$ . Right: “ $s_1t_2$ ” and “ $s_1t_1$ ” mean flows.

Unless otherwise stated, we focus on the amplitude of the magnetic field at location H ( $\{x, y, z\} = \{-109, 113, 0\}$  mm). Signals are recorded using National Instruments digitizers at a rate of 2000 Hz. In the remaining,  $\langle X \rangle$  stands for the time average of quantity  $X$ .

When driving the system in exact counter rotation ( $F_d = F_p$ ), a stationary dynamo state is reached via an imperfect supercritical bifurcation (as in [26,29]). The threshold is  $F_d = F_p \sim 17$  Hz. The time-averaged dynamo mode is axisymmetric and the profiles are similar to those observed with one soft-iron disk and one stainless steel disk [30]. The magnetic energy is four times larger in the probe shaft close to the disk than in the one close to the propeller; a feature that may lie in the specific dynamo mechanism in the immediate vicinity of the soft-iron disk [31,32].

### III. HYDRODYNAMIC BIFURCATION AND BISTABILITY

We first report on the hydrodynamic features when the disk and propeller are rotated asymmetrically. Figure 2(a) shows the evolution of the time-averaged total ( $\langle \Gamma_t \rangle = \langle \Gamma_d \rangle + \langle \Gamma_p \rangle$ ) and individual torques when the disk is driven at constant frequency ( $F_d = 13$  Hz), and the rotation of the propeller is progressively increased from exact counter rotation to a

very asymmetric driving ( $13 \leq F_p \leq 45$  Hz). Two branches are identified on  $\langle \Gamma_t \rangle$  as  $F_p$  exceeds 34 Hz. Upper values (H branch, filled symbols) correspond to the initial flow, while the lower ones (L branch, open symbols) correspond to a bifurcated flow reached when  $F_p$  exceeds 42 Hz. This bifurcation is associated with an increase of  $\langle \Gamma_p \rangle$  ( $\sim 10\%$ ) and a large decrease of  $\langle \Gamma_d \rangle$  ( $\sim 50\%$ ). When  $F_p$  is subsequently reduced, the L branch is explored down to  $F_p = 34$  Hz, for which it becomes unstable and the system jumps back to the H branch. The global behavior is hysteretic. Measurements repeated for several values of fixed  $F_d$  collapse when the time-averaged normalized torque difference  $\langle \Gamma_n \rangle$  is plotted as a function of the normalized rotation rate difference  $\Theta = (F_p - F_d)/(F_p + F_d)$ , as shown in Fig. 2(b), with  $\Gamma_n$  being defined as  $(\Gamma_p - \Gamma_d)/(\Gamma_p + \Gamma_d)$ . The transitions between the H and L branches are observed at  $\Theta_{LH} = 0.44$  and  $\Theta_{HL} = 0.53$ , within a  $\pm 0.01$  uncertainty. A typical time series of  $\Gamma_n$  at  $\Theta = \Theta_{LH}$  is shown in Fig. 4(b) for which the disk and propeller rotation rates are kept constant during the 60 s record displayed. A metastable state is observed at  $t < 15$  s, for which no evolution of  $\Gamma_n$  is observed before the flow bifurcates to the H branch at  $t \sim 15$  s (where  $\Gamma_n$  decreases).

The global bistable behavior of the hydrodynamic flow is confirmed by local velocity measurements. The hysteretic cycle of  $\langle v_\theta \rangle$  recorded by the potential probe, as  $F_p$  is varied while  $F_d$  is kept constant at 13 Hz, is displayed in Fig. 2(c). The value of  $\langle v_\theta \rangle$  is used as a proxy for the shear-layer location, as usually performed in von Kármán water flows [33]. In exact counter rotation,  $\langle v_\theta \rangle$  is positive; in the midplane the flow is dominated by the rotation imparted by the disk (and the shear layer is located closer to the propeller, in the  $x > 0$  region). As the rotation rate of the propeller is increased,  $\langle v_\theta \rangle$  decreases. When  $F_p \sim 30$  Hz,  $\langle v_\theta \rangle \simeq 0$  m s $^{-1}$  thus the shear layer is located in the midplane. The shear layer is pushed towards the disk (in the  $x < 0$  region) for higher values of  $F_p$ . When the flow has bifurcated in the L branch, the absolute value of  $\langle v_\theta \rangle$  is increased as compared to the H branch, and reaches the values measured when the flow is driven by the rotation of the propeller alone ( $F_d = 0$ ). The local velocity measurements thus show that the H branch is associated with an “ $s_1t_2$ ” flow, whereas the bulk flow of the L branch corresponds to an “ $s_1t_1$ ” flow (for  $0 < F_d \ll F_p$ , a counter-rotating layer is always localized in the vicinity of the disk [4,33]). While similar

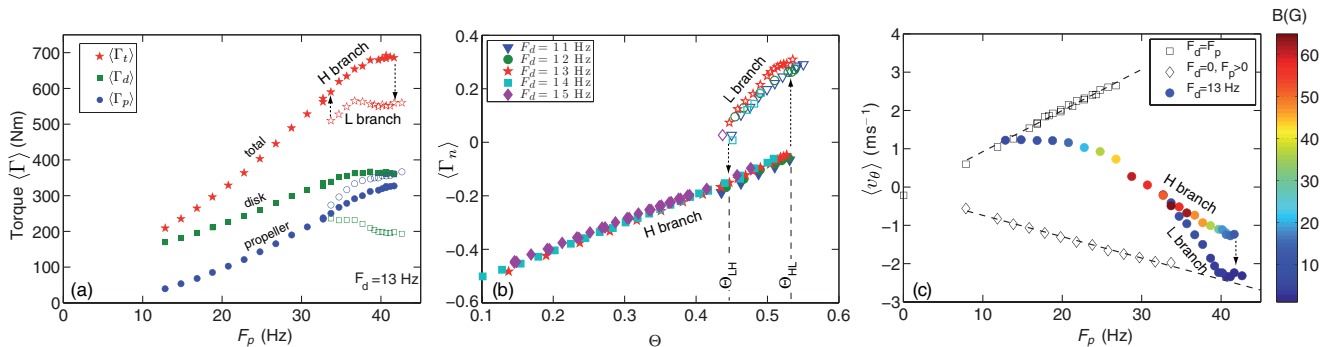


FIG. 2. (Color online) (a) Evolution of time-averaged torques as a function of  $F_p$  for  $F_d = 13$  Hz. (b) Evolution of  $\langle \Gamma_n \rangle$  as a function of  $\Theta$ . (c) Evolution of  $\langle v_\theta \rangle$  as a function of  $F_p$ . (•)  $F_d = 13$  Hz (colors stand for the amplitude of the magnetic field, see Fig. 3). (□) Values at exact counter rotation  $F_d = F_p$ . (◇) Values for propeller rotation only ( $F_d = 0$ ).

subcritical bifurcations and multistability have already been observed in confined turbulent flows [4–8], the relevant feature here is that it occurs between MHD flows that are capable of dynamo action.

**IV. DYNAMO BEHAVIOR**

Let us now investigate the evolution of the magnetic field strength  $B = \sqrt{\langle B_x^2 \rangle + \langle B_y^2 \rangle + \langle B_z^2 \rangle}$ , as a function of the asymmetry parameter  $\Theta$ , as shown in Fig. 3(a). We first focus on star symbols, for which  $F_d = 13$  Hz. Increasing the propeller velocity, i.e., increasing  $\Theta$ , the H-branch flow generates a dynamo. As  $\Theta$  increases, the magnetic field increases and then saturates. Eventually  $B$  decreases as  $\Theta$  reaches its highest values in the H branch (where  $\Gamma_d$  saturates). For  $\Theta = \Theta_{HL}$ , the flow bifurcates to the L branch and  $B$  drops to very low values. When  $\Theta$  is subsequently reduced, the magnetic behavior follows the (hysteretic) dynamics of the hydrodynamic bifurcation, with values lower than 4 G (open symbols). The bistable magnetic behavior has been observed for all investigated rotation rates of the disk  $F_d$  [see Fig. 3(a)]. An interesting feature of the magnetic behavior is observed for  $\Theta$  values close to  $\Theta_{LH}$ . Figure 3(b) displays the evolution of  $B$  as a function of  $F_d$  for both stationary H and L branches at  $\Theta = 0.46$  (full lines). A dynamo bifurcation is clearly observed for the H-branch flow. The amplitude of  $B$  sharply increases with  $F_d$ , leading to a dynamo onset  $F_d \sim 12$  Hz. As already described, the magnetic field measured in the L

branch is lower, but also sharply increases nonlinearly with  $F_d$  to reach 6 G at  $F_d = 14$  Hz. While induction as high as eight times the applied field were observed in Taylor-Couette flow at similar Rm [34] (and linearly scaling with Rm [35]), in the VKS experiment, the maximum magnetic field resulting from ambient field amplification is generally much smaller than the values reported here for the L branch [36]. Unfortunately, due to motor power limitations, no stationary fixed points were accessible in the L branch above  $F_d = 14$  Hz. It is then instructive to analyze the magnetic behavior at  $\Theta = \Theta_{LH}$ , in the metastable state before the transition to the H branch. The evolution of  $B$  as a function of  $F_d$  is displayed as a dashed line in Fig. 3(b). When  $F_d \leq 14$  Hz, the magnetic field amplitude at  $\Theta_{LH}$  accurately represents that of the stationary L-branch points at  $\Theta = 0.46$  [red full line in Fig. 3(b)]. For  $F_d = 15$  Hz, the magnetic field amplitude at  $\Theta = \Theta_{LH}$  reaches 15 G (measured at the early stage of the hydrodynamical transition to the H branch). This amplitude suggests that the stationary L branch could lead to a dynamo branch with a threshold  $F_d$  around 14 Hz at  $\Theta = 0.46$  (with magnetic field amplitudes comparable to low amplitude dynamos previously reported in the VKS experiment [29]). Due to the experimental limitations,

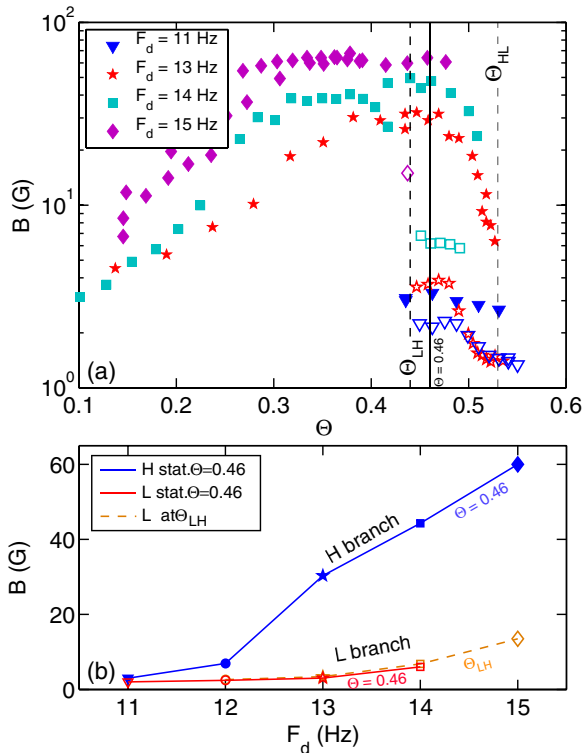


FIG. 3. (Color online) (a) Amplitude of the magnetic field  $B$  as a function of  $\Theta$  for four values of  $F_d$ . Full symbols for H branch and open symbols for L branch. (b) Stationary points in the L and H branches at  $\Theta = 0.46$  (full lines) and points at  $\Theta = \Theta_{LH}$  (dashed line). See text for details.

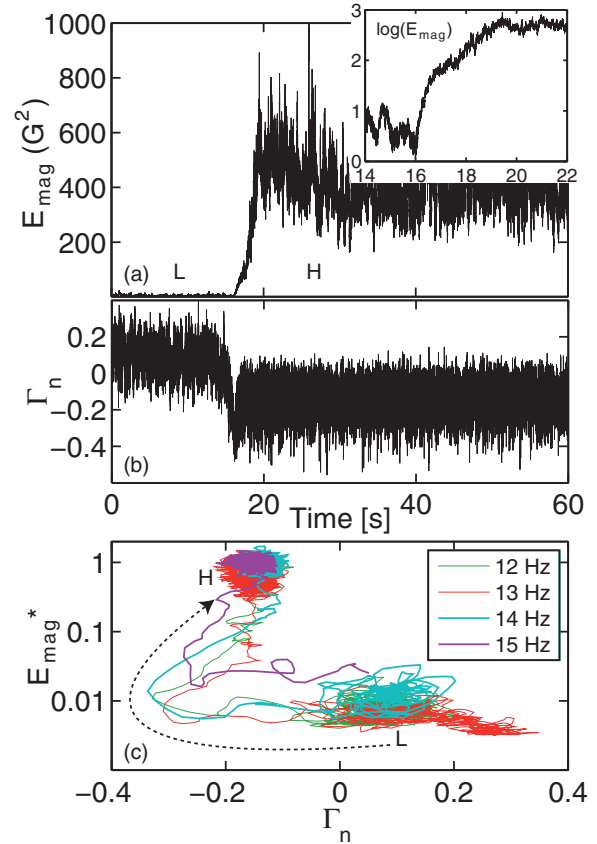


FIG. 4. (Color online) Time series of (a)  $E_{mag}$  and zoom in logarithmic units (inset) and (b)  $\Gamma_n$  at L-H transition ( $F_d = 14$  Hz,  $F_p = 37$  Hz). Growing times  $t_s$  and  $t_l$  decrease from 0.41 s to 0.18 s and 0.05 s, and 1.4 s to 1 s and 0.4 s, respectively, when  $F_d$  is increased from 13 to 15 Hz. (c) Phase-space  $E_{mag}^*$  ( $\Gamma_n$ ) at  $\Theta = \Theta_{LH}$ . Signals averaged over 0.25 s.

the determination of the exact nature of the dynamo bifurcation in the L branch requires further investigations.

As a partial conclusion, each of the two bistable flow configurations are shown to have a different magnetic behavior. For the same rotation rate of the soft-iron disk  $F_d$  around 13 Hz, a high-field dynamo coexists with no dynamo, depending on the flow configuration.

## V. DYNAMICS OF THE L-H TRANSITIONS

A last point concerns the dynamics of the transitions between the two branches at  $\Theta = \Theta_{LH}$  and  $\Theta = \Theta_{HL}$ . This dynamics is characterized by the fact that the hydrodynamic bifurcation between the two flows is subcritical, whereas the dynamo bifurcates supercritically. We will thus focus on regimes close to the H-branch dynamo onset. Simultaneous time series of the magnetic energy  $E_{\text{mag}}$  and  $\Gamma_n$  during the L to H transition are displayed in Figs. 4(a) and 4(b). The magnetic energy is defined as the mean over all sensors,  $E_{\text{mag}}(t) = 1/40 \sum_{i=1}^{40} [B_{i,x}(t)^2 + B_{i,y}(t)^2 + B_{i,z}(t)^2]$ . While  $\Theta$  is kept constant during the 60 s record, the system switches from the L branch to the H branch at time  $t \sim 15$  s, where  $\Gamma_n$  decreases and  $E_{\text{mag}}$  increases. As shown in the inset of Fig. 4(a), the (fluctuating) magnetic energy exponentially increases, first with a short characteristic time  $t_s$ , then with a longer characteristic time  $t_l$ . We note that  $t_l$  is of the order of the magnetic diffusion time over the flow size, while  $t_s$  is an order of magnitude smaller.

Complementary information about the L-H transition dynamics comes from its trajectory in phase space where a normalized magnetic energy  $E_{\text{mag}}^* = E_{\text{mag}} / \langle E_{\text{mag}} \rangle_H$  (where  $\langle E_{\text{mag}} \rangle_H$  is the time-averaged magnetic energy in the H branch) is plotted as a function of  $\Gamma_n$ , as displayed in Fig. 4(c). A similar dynamics during the L to H transitions (at  $\Theta = \Theta_{LH}$ ) for the four values of  $F_d$  above the H-branch dynamo threshold has been observed. The transition initially follows a trajectory at constant magnetic energy and decreasing  $\Gamma_n$ . After a (negative) overshoot of  $\Gamma_n$ , the magnetic energy increases

at nearly constant  $\Gamma_n$ . It is thus clear that the magnetic bifurcation between the L and H branches is triggered by the hydrodynamic bifurcation, and that the magnetic energy evolution is always delayed.

## VI. CONCLUSION AND DISCUSSION

In the sodium flows studied here—capable of dynamo action—a high-field dynamo branch (associated with an “ $s_1 t_2$ ”-type flow) coexists with a low-field branch (associated with an “ $s_1 t_1$ ”-type flow) for the same experimental control parameters. While dynamo bifurcation between branches with different magnetic field amplitudes and different flow geometries is a long-standing issue in dynamo research, it must be stressed that the transition is observed here as the sole consequence of a turbulent hydrodynamic bifurcation, also observed below the dynamo threshold. In the present experiment, no influence of the Lorentz force on flow bistability has been observed. The reason lies in the fact that the transition between the two flows is subcritical whereas the magnetic field bifurcates supercritically. The Lorentz force that saturates the magnetic field above the dynamo threshold being small, it is unable to trigger a transition between the two well-separated hydrodynamic attractors. An increase of available mechanical power would allow more intense driving of the flow by the soft-iron disk, and thus larger dynamo magnetic fields which might modify the hydrodynamic bifurcation.

## ACKNOWLEDGMENTS

We thank S. Aumaître for his participation in the experimental runs and N. Bonnefoy, M. Moulin, C. Gasquet, A. Skiara, D. Courtiade, J.-F. Point, P. Metz, V. Padilla, and M. Tanase for their technical assistance. This work was supported by ANR 08-0039-02, Direction des Sciences de la Matière, and Direction de l’Énergie Nucléaire of CEA, Ministère de la Recherche, and CNRS. The experiment is performed at CEA/Cadarache DEN/DTN.

- 
- [1] M. Schmeits and H. Dijkstra, *J. Phys. Oceanogr.* **31**, 3435 (2001).
  - [2] O. R. Burrgraf and M. R. Foster, *J. Fluid Mech.* **80**, 685 (1977).
  - [3] R. Labbé, J. F. Pinton, and S. Fauve, *Phys. Fluids* **8**, 914 (1996).
  - [4] F. Ravelet, L. Marié, A. Chiffaudel, and F. Daviaud, *Phys. Rev. Lett.* **93**, 164501 (2004).
  - [5] A. de la Torre and J. Burguete, *Phys. Rev. Lett.* **99**, 054101 (2007).
  - [6] B. Saint-Michel, B. Dubrulle, L. Marié, F. Ravelet, and F. Daviaud, *Phys. Rev. Lett.* **111**, 234502 (2013).
  - [7] G. Ahlers, S. Grossmann, and D. Lohse, *Rev. Mod. Phys.* **81**, 503 (2009).
  - [8] D. A. Zimmerman, S. A. Triana, and D. P. Lathrop, *Phys. Fluids* **23**, 065104 (2011).
  - [9] P. H. Roberts, *Rotating Fluids in Geophysics* (Academic, New York, 1978).
  - [10] U. R. Christensen, P. Olson, and G. A. Glatzmaier, *Geophys. J. Int.* **138**, 393 (1999).
  - [11] B. Sreenivasan and C. A. Jones, *J. Fluid Mech.* **688**, 5 (2011).
  - [12] R. D. Simitev and F. H. Busse, *Europhys. Lett.* **85**, 19001 (2009).
  - [13] V. Morin and E. Dormy, *Int. J. Mod. Phys. B* **23**, 5467 (2009).
  - [14] Y. Ponty, J. P. Laval, B. Dubrulle, F. Daviaud, and J. F. Pinton, *Phys. Rev. Lett.* **99**, 224501 (2007).
  - [15] G. Krstulovic, G. Thorner, J. P. Vest, S. Fauve, and M. Brachet, *Phys. Rev. E* **84**, 066318 (2011).
  - [16] F. Rincon, G. I. Ogilvie, and M. R. E. Proctor, *Phys. Rev. Lett.* **98**, 254502 (2007).
  - [17] B. Dubrulle, P. Blaineau, O. Mafra Lopes, F. Daviaud, J.-P. Laval, and R. Dolganov, *New J. Phys.* **9**, 308 (2007).
  - [18] A. K. Gailitis *et al.*, *Phys. Rev. Lett.* **84**, 4365 (2000).
  - [19] R. Stieglitz and U. Müller, *Phys. Fluids* **13**, 561 (2001).
  - [20] R. Monchaux *et al.*, *Phys. Rev. Lett.* **98**, 044502 (2007).
  - [21] M. Berhanu *et al.*, *J. Fluid Mech.* **641**, 217 (2009).
  - [22] F. Pétrélis and S. Fauve, *J. Phys.: Condens. Matter* **20**, 494203 (2008).
  - [23] M. L. Dudley and R. W. James, *Proc. Roy. Soc. A Math. Phys.* **425**, 407 (1989).

- [24] N. L. Peffley, A. B. Cawthorne, and D. P. Lathrop, *Phys. Rev. E* **61**, 5287 (2000).
- [25] E. J. Spence, M. D. Nornberg, C. M. Jacobson, R. D. Kendrick, and C. B. Forest, *Phys. Rev. Lett.* **96**, 055002 (2006).
- [26] R. Monchaux *et al.*, *Phys. Fluids* **21**, 035108 (2009).
- [27] T. Kumaresan and J. B. Joshi, *Chem. Eng. J.* **115**, 173 (2006).
- [28] V. Noskov, R. Stepanov, S. Denisov, P. Frick, G. Verhille, N. Plihon, and J.-F. Pinton, *Phys. Fluids* **21**, 045108 (2009).
- [29] M. Berhanu *et al.*, *Eur. Phys. J. B* **77**, 459 (2010).
- [30] J. Boisson *et al.*, *New J. Phys.* **14**, 013044 (2012).
- [31] G. Verhille, N. Plihon, M. Bourgoin, Ph. Odier, and J.-F. Pinton, *New J. Phys.* **12**, 033006 (2010).
- [32] A. Giesecke, C. Nore, F. Stefani, G. Gerbeth, J. Léorat, W. Herreman, F. Luddens, and J.-L. Guermond, *New J. Phys.* **14**, 053005 (2012).
- [33] P.-P. Cortet, P. Diribarne, R. Monchaux, A. Chiffaudel, F. Daviaud, and B. Dubrulle, *Phys. Fluids* **21**, 025104 (2009).
- [34] S. A. Colgate *et al.*, *Phys. Rev. Lett.* **106**, 175003 (2011).
- [35] V. I. Pariev, S. A. Colgate, and J. M. Finn, *Astrophys. J.* **658**, 129 (2007).
- [36] S. Miralles *et al.*, *Phys. Rev. E* **88**, 013002 (2013).